Regenerative Therapy 15 (2020) 77–89

Contents lists available at ScienceDirect

Regenerative Therapy

journal homepage: http://www.elsevier.com/locate/reth

Original Article

Osteochondral regeneration using scaffold-free constructs of adipose tissue-derived mesenchymal stem cells made by a bio three-dimensional printer with a needle-array in rabbits

Daiki Murata [a, b, *], Yoshihiro Kunitomi [c], Kaori Harada [c], Satoshi Tokunaga [d, e], Shoko Takao [b], Koichi Nakayama [b]

[a] Veterinary Surgery, Department of Veterinary Clinical Science, Joint Faculty of Veterinary Medicine, Kagoshima University, Kagoshima, Japan
[b] Center for Regenerative Medicine Research, Faculty of Medicine, Saga University, Saga, Japan
[c] Cyfuse Biomedical K.K., 3-1 Hongo 7-chome, Bunkyo-ku, Tokyo, Japan
[d] Veterinary Teaching Hospital, Joint Faculty of Veterinary Medicine, Kagoshima University, Kagoshima, Japan
[e] Veterinary Teaching Hospital, College of Veterinary Medicine and Biomedical Science, Colorado State University, Fort Collins, CO, USA

ARTICLE INFO

Article history:
Received 3 September 2019
Received in revised form
24 April 2020
Accepted 3 May 2020

Keywords:
Bio 3D printer
Scaffold-free
Cartilage regeneration
Osteochondral regeneration
Mesenchymal stem cells

ABSTRACT

Osteoarthritis is a major joint disease for which medical interventions have been extensively investigated in humans and animals. In this study, we examined the regeneration of articular cartilage and subchondral bone using a scaffold-free construct consisting of adipose tissue-derived mesenchymal stem cells (AT-MSCs) fabricated using a bio three-dimensional (3D) printer. AT-MSCs were isolated from three rabbits and cultured to a number of sufficient for creation of 3D-printed constructs. One construct consisted of 960 spheroids obtained from 3.5×10^4 autologous AT-MSCs. The construct was then implanted into an osteochondral defect (diameter 4 mm and depth 4 mm) surgically bored into the left femoral trochlear groove of each rabbit. Three months after implantation, healing was assessed by computed tomography, magnetic resonance (MR) imaging, and pathology. MR images were evaluated based on a modified two-dimensional (2D)-magnetic resonance observation of cartilage repair tissue (MOCART) grading system, and gross and microscopic histology were scored according to the International Cartilage Repair Society scale. At the time of imaging, treated defects had become radiopaque, while control defects remained radiolucent. Total 2D-MOCART scores were higher in the implanted defects than in the controls, but not to a statistically significant extent. Similarly, average histological scores were comparable among all groups, although average gross scores were significantly higher in implanted defects than in controls. This is the first demonstration of a scaffold-free 3D-printed construct consisting of autologous AT-MSCs regenerating cartilage and subchondral bone within three months.

1. Introduction

Osteoarthritis, defined as cartilage degradation and subchondral bone sclerosis/deformity, is a major joint disease that contributes to midlife and geriatric locomotor deficiency [1]. The disease slowly progresses with the accumulation of bone, cartilage, and ligament damage [2], and the associated disability may decrease quality of life [3]. In advanced stages, cartilage degeneration and subchondral bone sclerosis are exacerbated even by the usual mechanical load of daily activities [2]. Therefore, surgical strategies that reconstruct both bone and cartilage to restore joint structure and function have been investigated in such cases [4].

Although osteochondral autografts promote favorable outcomes following surgery [5], the loss of clinically sound cartilage is inevitable, and an amount of autografts is limited by the size of the osteochondral defects [6]. Alternatively, combinations of artificial bone and autologous chondrocytes seeded onto collagen scaffolds promote bone and cartilage restoration [7,8]. However, such

* Corresponding author. Center of Regenerative Medicine Research, Faculty of Medicine, Saga University, Honjo-machi, Saga, 840-8502, Japan.
E-mail address: daiki_net_official@yahoo.co.jp (D. Murata).
Peer review under responsibility of the Japanese Society for Regenerative Medicine.

https://doi.org/10.1016/j.reth.2020.05.004

implants require isolation of a small number of chondrocytes from a large amount of normal cartilage. In addition, these cells may dedifferentiate by during passage in culture [7,9]. To overcome these issues, bone and cartilage regeneration from stem cells has been attempted [10]. Indeed, mesenchymal stem cells (MSCs) derived from bone marrow, adipose tissue (AT), synovium, synovial fluid, umbilical cord tissue, and umbilical cord blood have been shown to differentiate into bone and cartilage *in vitro* [11–16]. Of these, AT is easily obtained by liposuction under local anesthesia. Furthermore, adipose tissue-derived mesenchymal stem cells (AT-MSCs) can be effectively collected from the tissue, and those isolated from a mature animal are known to maintain high growth rates [17,18]. Therefore, AT appear to be the most feasible source of MSCs.

Although MSCs can be grown *in vitro* as two-dimensional (2D) monolayers using conventional tissue culture technology, this technique does not provide a suitable microenvironment [19]. Thus, three-dimensional (3D) culture techniques have been developed in recent years to reproduce tissue morphology, to facilitate intercellular adhesion and interaction via the extracellular matrix, and to enhance multilineage differentiation potential [20]. In addition, the expression of genes and molecules related to angiogenesis and wound healing is promoted in 3D cultures of rabbit AT-MSCs [21].

Remarkably, new native bone can be produced after the implantation of bone-like scaffolds, such as those composed of beta-tricalcium phosphate, with or without bone-inducing factors, because osteoclasts eventually degrade such implants and osteoblasts regenerate the original bone matrix. On the other hand, articular cartilage lacks the ability to degrade artificial scaffolds because of its lower self-restorative capacity, avascularity, and hypocellularity. Therefore, we hypothesized that scaffold-free 3D implants consisting entirely of cells would be more suitable for regenerating articular cartilage.

Indeed, implantation of scaffold-free 3D constructs consisting of AT-MSCs elicited bone and cartilage regeneration at osteochondral defects in rabbits and pigs [22–25]. These constructs were fabricated by manually stacking spheroids into a cylindrical mold. More sophisticated constructs with pre-defined shapes, densities, and distributions of spheroids have also been generated by bio 3D printing [25,26]. Notably, bio 3D printed materials have higher elasticities than do manual constructs and are easier to manipulate during implantation. Most importantly, these materials can be customized precisely to match the size and shape of various osteochondral defects.

In this study, we fabricated three constructs on a bio 3D printer. These constructs were then implanted into osteochondral defects, and healing was assessed after three months using computed tomography (CT) and magnetic resonance (MR) imaging. Gross and histological features were also scored according to the ICRS grading system.

2. Materials and methods

2.1. Animals

Six mature male New Zealand White rabbits (Kitayama Labs K.K., Nagano, Japan) with mean weight 4.21 kg (ranging from 3.91 to 4.69 kg) were divided into two groups of three rabbits each. One group was left untreated after surgical injury, while the other was implanted with the bio 3D printed constructs. All procedures were evaluated and approved by the Institutional Animal Care and Use Committee in LSI Medience Corporation (Application No. P130912; Approval No. 2013–0706).

2.2. Isolation and expansion of adipose tissue-derived mesenchymal stem cells

Cervical AT (15–30 g per animal) was aseptically collected under general anesthesia, minced, and digested for 3 h in phosphate-buffered saline (PBS) containing 0.1% collagenase (Collagenase L; Nitta Gelatin, Osaka, Japan). The digests were filtered through a 100 μm pore membrane (Cell Strainer; BD Biosciences, Franklin Lakes, NJ, USA), and centrifuged at 190×*g* for 5 min at room temperature. After removing the resulting supernatant, the pellet was resuspended in complete culture medium (CCM) consisting of Dulbecco's Modified Eagle's Medium (DMEM; Life Technologies, Carlsbad, CA, USA), 10% fetal bovine serum (FBS; GE Healthcare, Little Chalfont, UK), and 1% antibiotics (100 U/mL penicillin G and 100 μg/mL streptomycin; Pen Strep; Life Technologies). The cells were centrifuged a second time, resuspended in fresh CCM, and seeded in 75 cm^2 culture flasks (Cell Culture flask; Corning Inc., NY, USA). Following incubation at 37 °C with 5% CO_2 for 4–5 days, adherent cells were washed with PBS and cultured in fresh CCM as passage 0. The medium was changed every other day. Nine days after seeding, the cells were harvested with recombinant trypsin (TrypLE Select; Life Technologies), diluted with an equal volume of fresh CCM, and centrifuged. After removal of the resulting supernatant, the pellet was rinsed with CCM, seeded at 3.0×10^6 cells per 225 cm^2 flask (Corning), and cultured until 90% confluence with a change of medium every other day. This process was repeated four times until passage five to obtain a sufficient number of cells for construct preparation.

2.3. Tri-lineage differentiation

To investigate osteogenic differentiation, the AT-MSCs were placed in a 6-well plate (Nunc Cell-Culture Treated Multidish, Thermo Fisher Scientific K.K., Tokyo, Japan) in CCM at an initial density of 3.0×10^4 cells/well. After 24 h of incubation, the medium was changed with osteogenic induction medium (Differentiation Basal Medium-Osteogenic; Lonza, Walkersville, MD), supplemented with 100 μM ascorbic acid, 10 mM β-glycerophosphate, and 1 μM dexamethasone, for four weeks. To investigate chondrogenic differentiation, AT-MSCs (3×10^4) were resuspended in a 6-well plate in CCM. After incubation for 24 h, the medium was replaced with chondrogenic induction medium (Differentiation Basal Medium-Chondrogenic, Lonza), supplemented with 4.5 g/L D-glucose, 350 μM L-proline, 100 nM dexamethasone, and 0.02 g/L transforming growth factor beta 3. Chondrogenic differentiation was induced in plate cultures for two weeks. Adipogenic differentiation began when AT-MSCs attached to the bottom of a 6-well plate at a density of 2×10^5 cells/well in CCM. Following a 24 h pre-incubation, the medium was replaced with Adipogenic Induction Medium (Lonza), supplemented with 4.5 g/L D-glucose, 100 μM indomethacin, 10 μg/mL insulin, 0.5 mM 3-isobutyl-1-methylxanthine, and 1 μM dexamethasone for one week. As negative control of osteogenic, chondrogenic, and adipogenic differentiation, AT-MSCs were cultured in CCM for four weeks, two weeks, and one week, respectively.

Moreover, to investigate tri-linage differentiation after AT-MSCs formed a spheroid, the cells (1×10^6) were resuspended in a 15-mL culture tube (SuperClear centrifuge tubes; Labcon, Petaluma, CA) in 1 mL of osteogenic, chondrogenic, and adipogenic induction medium (Lonza). Tri-linage differentiation was induced in pellet cultures for 3 weeks. Each cell pellet was fixed with 10% neutral buffered formalin (NBF), embedded in paraffin, and cut into 5 μm sections using a microsection instrument.

Production of calcium apatite crystals in the osteogenic extracellular matrix was evaluated with alizarin red staining in the wells

of culture plates. Cartilage-specific proteoglycans were stained with alcian blue or toluidine blue, and adipocyte-specific intracellular lipids were stained with oil red O.

2.4. Bio 3D printing

At least 3.5×10^7 autologous AT-MSCs were used to fabricate each construct as previously described [25,26]. Briefly, cells were inoculated into 10 96-well low-adhesion plates (PrimeSurface 96U Plate; Sumitomo Bakelite, Tokyo, Japan) at 3.5×10^4 cells/well. After static incubation for 48 h, the cells formed spheroids with diameters of approximately 600 μm (Fig. 1a).

A bio 3D printer (Regenova; Cyfuse Biomedical K.K., Tokyo, Japan) was used to assemble the spheroids into scaffold-free tubular tissues pre-designed with the bio 3D design software (B3D; Cyfuse Biomedical K.K.). The printer was fitted with an array of needles with diameter 0.17 mm, interval between needles 0.4 mm, and total useable size 3.2 mm square × 10 mm high (Fig. 1b and c). To assemble the construct, 960 spheroids were individually picked up from the 96-well plates by a robotically controlled, 26-gage fine suction nozzle (outer diameter 0.46 mm, inner diameter 0.25 mm) and stacked inside needles. This process took approximately 2.5 h (Fig. 1b and c). The needle array was then placed in a perfusion chamber and cultured at 37 °C with 5% CO_2 for six days to fuse the spheroids to one another. After extrication from the needle array, a construct was obtained with diameter 4 mm and height 4 mm. These constructs were then implanted autologously one day after extrication (Fig. 1d and e).

2.5. Cell viability

Cell viability in constructs, spheroids, and 2D cultures was assessed by flow cytometry. Briefly, 3D constructs were dispersed into single cells by digestion at 37 °C for 140 min with 4 mg/mL collagenase (Collagenase Type I; Worthington Biochemical, Lake wood, NJ, USA). The cells (1×10^6) were then washed with PBS, resuspended in 100 μL PBS containing 1% FBS, and stained for 5 min in the dark with 1 μL of 1 mg/mL propidium iodide (PI; Sigma–Aldrich, St. Louis, MO, USA). Unstained cells were used as a negative control. Cells were sorted with a flow cytometer (FACSVerse™, BD Bioscience), and cell viability was calculated as the percentage of cells unstained by PI.

2.6. Histology of cell construct

One of the constructs was fixed in 10% NBF for 1 week and embedded in paraffin. Serial sections (5 μm thick) were placed on glass slides and stained with hematoxylin and eosin (HE), Elastica Masson, and by immunohistochemistry using specific mouse antibodies against human collagen type I (Anti Collagen I; Southern Biotechnology Associates, Birmingham, AL, USA) and an avidin–biotin complex system (VECTASTAIN ABC Standard Kit; Vector Laboratories, Southfield, MI, USA).

2.7. Implantation

Animals were pre-treated with sedatives (intramuscular injections of 50 μg/kg medetomidine and 250 μg/kg midazolam) and analgesics (intramuscular injections of 100 μg/kg butorphanol and 5 mg/kg ketamine). Constructs were then implanted into surgically created defects under general anesthesia using oxygen, nitrogen monoxide, and isoflurane. Briefly, the femoropatellar joint was incised to expose the femoral trochlear groove. Using a surgical trephine with an outer diameter of 4.8 mm (Cancellous Collector; Sophia Tech, Tokyo, Japan), the articular cartilage and subchondral bone were drilled to a depth of 4 mm at the center of the groove in the left hind limbs (Fig. 2a and b). The defects were then implanted autologously with the constructs (Fig. 2a) or left untreated in control animals (Fig. 2b).

2.8. Computed tomography imaging

Osteochondral defects were imaged three months after surgery with a CT scanner (Aquilion LB; Toshiba, Tokyo, Japan). In brief,

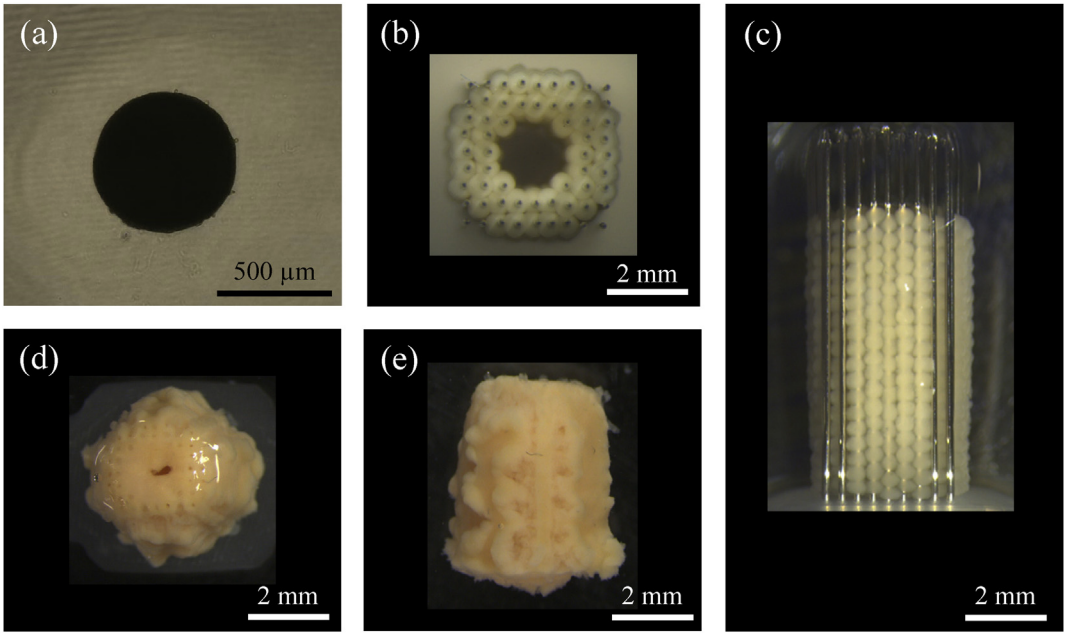

Fig. 1. Preparation of spheroids and 3D constructs. (a) A representative cell spheroid approximately 600 μm in diameter for use in fabricating a construct by bio 3D printing. (b and c) A columnar construct (4 mm in diameter, upper view; 4 mm in height, side view) immediately after stacking spheroids into a needle array. (d and e) A columnar construct (upper view and side view) extricated from the needle array six days after culture. Scale bar = 500 μm (a) and 2 mm (b–e).

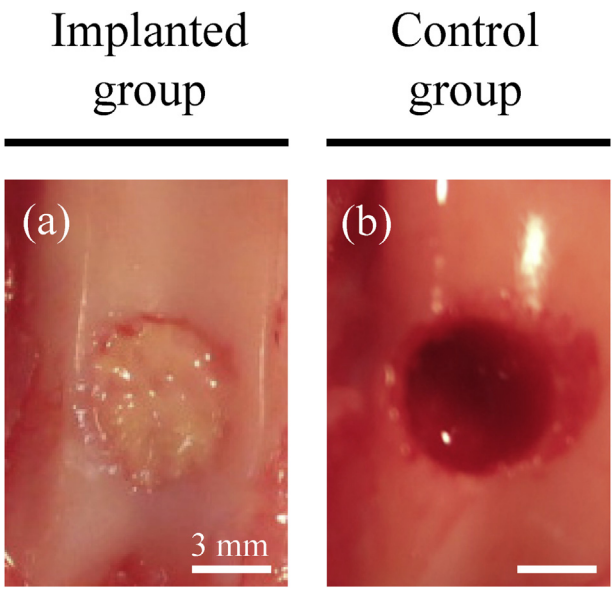

Fig. 2. Surgical implantation. (a) A cylindrical osteochondral defect was surgically bored into each groove of the left hind limb before implantation with autologous bio 3D-printed constructs. (b) Untreated defects were used as controls. Scale bars = 3 mm (a and b).

animals were sedated by intramuscular injection of 50 μg/kg medetomidine and 250 μg/kg midazolam, anesthetized using isoflurane as described in section 2.5, and restrained in a dorsal position. The left stifles were then serially imaged by CT and two- and three-dimensionally reconstructed in conjunction with MR images. Fig. 4 depicts longitudinal sections of 0.5 mm obtained in lateral view.

2.9. Magnetic resonance imaging

Osteochondral defects were also evaluated three months after surgery by imaging the left stifle with a 3.0 T MR system (Trillium Oval; Hitachi, Tokyo, Japan). After CT in the dorsal position, animals were imaged in a coil intended for human imaging. Subsequently, proton density (PD)-MR images were scored based on a modified 2D-magnetic resonance observation of cartilage repair tissue (MOCART) scale (Table 1).

2.10. Pathology

All rabbits were euthanized by intravenous overdose of pentobarbital sodium after CT and MR imaging, and gross features were blindly scored using International Cartilage Repair Society (ICRS) scale (Table 2). Both distal femurs were then fixed in 10% NBF, longitudinally sectioned parallel to the trochlear groove, decalcified with a chelating agent (K-CX; Falma, Tokyo, Japan), and embedded in paraffin. Subsequently, serial sections (5 μm) were obtained, placed on glass slides, and stained with HE and safranin O. For immunohistochemistry, sections were probed with 5 μg/mL antibodies against collagen type II (Novus Biologicals, Littleton, CO, USA), labeled with biotin-conjugated goat anti-mouse IgG (Vector Laboratories), and incubated with peroxidase-conjugated streptavidin (Nichirei, Tokyo, Japan) for 5 min. Finally, specimens were visualized with diaminobenzidine, counterstained with Mayer's hematoxylin (Muto Pure Chemicals, Tokyo, Japan), and scored according to the ICRS scale (Table 3).

2.11. Statistical analysis

All numeric data are reported as means ± standard deviation (SD). 2D-MOCART and ICRS scores were compared between the implanted and control groups with the *t*-test and $p < 0.05$ was considered statistically significant.

3. Results

3.1. Tri-lineage potential

Rabbit AT-MSCs adhering to the bottom of the culture dish were spindle-shaped and proliferated well. Following osteogenic induction, AT-MSCs showed appropriate characteristics of osteocytes, including staining with alizarin red, indicating the presence of calcium apatite crystals (Fig. 3a), and compared with negative control (Fig. 3b). AT-MSCs were round-shaped and showed a sheet-shaped structure that was positively stained with alcian blue (Fig. 3c). On the other hand, the cells didn't form sheet-shaped and only their nucleuses were stained with alcian blue (Fig. 3d). Adipogenic induction of the AT-MSCs resulted in adipocyte-like flattened cells with small lipid vesicles that were positively stained with oil red O (Fig. 3e). No stained vesicles were observed in a negative control (Fig. 3f).

Histological observation of the cell pellets also indicated calcium apatite crystals stained with alizarin red after osteogenic induction (Fig. 4a), showed a hyaline cartilage structure stained with toluidine blue after chondrogenic induction (Fig. 4c), and contained lipid droplets stained with oil red O after adipogenic induction (Fig. 4e). On the other hand, no stained materials were observed in a negative control (Fig. 4b, d, and f).

3.2. Cell viability

Cell viability was measured by flow cytometry as the percentage of cells not stained with PI (Fig. 5). In 2D cultures, almost all cells were viable (97.8%; Fig. 5a), while 97.0% of cells were viable in spheroids (Fig. 5b). In constructs, 86.3% of cells were viable (Fig. 5c).

3.3. Histology of cell construct

Microscopic observation of the cell construct is presented in Fig. 6. The boundaries of the spheroids were unclear and tended to agglutinate with each other (Fig. 6a, b, and c). Numerous cell nuclei were confirmed inside and around the spheroids (Fig. 6a, b, and c), and ECM production was observed but not specifically within the construct in the section stained with Elastica Masson (Fig. 6d, e, and f). Furthermore, the section stained by immunohistochemistry for collagen type I was positive in correspondence with Elastica Masson staining (Fig. 6g, h, and i).

3.4. Computed tomography imaging

Representative CT images are shown for each group in Fig. 7a and b. In implanted rabbits, a radiopaque material had emerged from and bridged the boundary between bone and construct (Fig. 7a). In contrast, a radiolucent area persisted in control animals (Fig. 7b).

3.5. Magnetic resonance imaging and modified 2D-magnetic resonance observation of cartilage repair tissue scores

Representative PD-MR images are shown in Fig. 5c and d. These images indicate that the articular cartilage in implanted animals had been restored to a state near that of surrounding uninjured

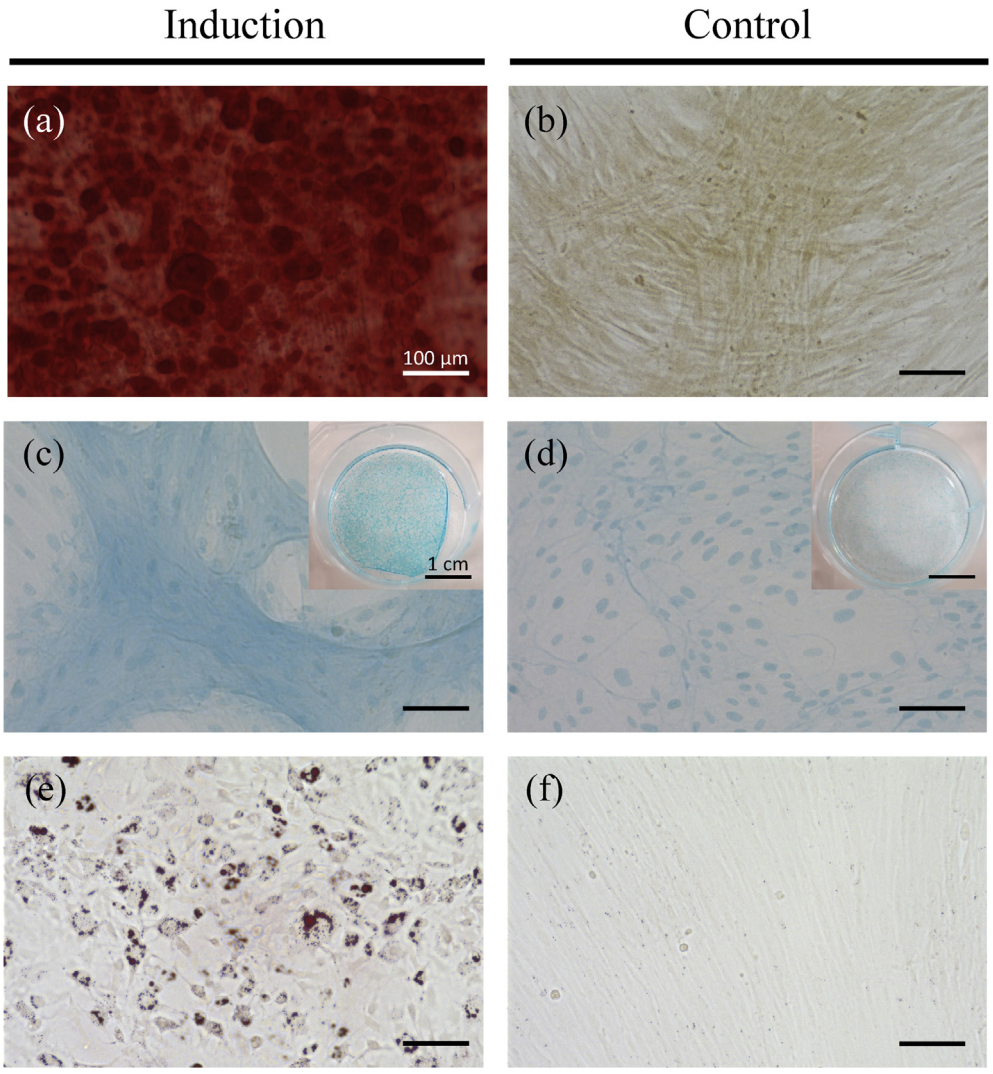

Fig. 3. Tri-linage differentiation of AT-MSCs. (a) Calcium apatite stained with alizarin red in osteogenic induction (b) AT-MSCs slightly stained orange with alizarin red in negative control. (c) A sheet-shaped structure positively stained with alcian blue in chondrogenic induction. (d) No sheet-shaped structure and their nucleuses stained with alcian blue in negative control. (e) The MSCs with small lipid vesicles stained positively with oil red O in adipogenic induction. (f) No stained vesicles in a negative control. Scale bars = 100 μm (a–f) and 1 cm (Insets of c and d).

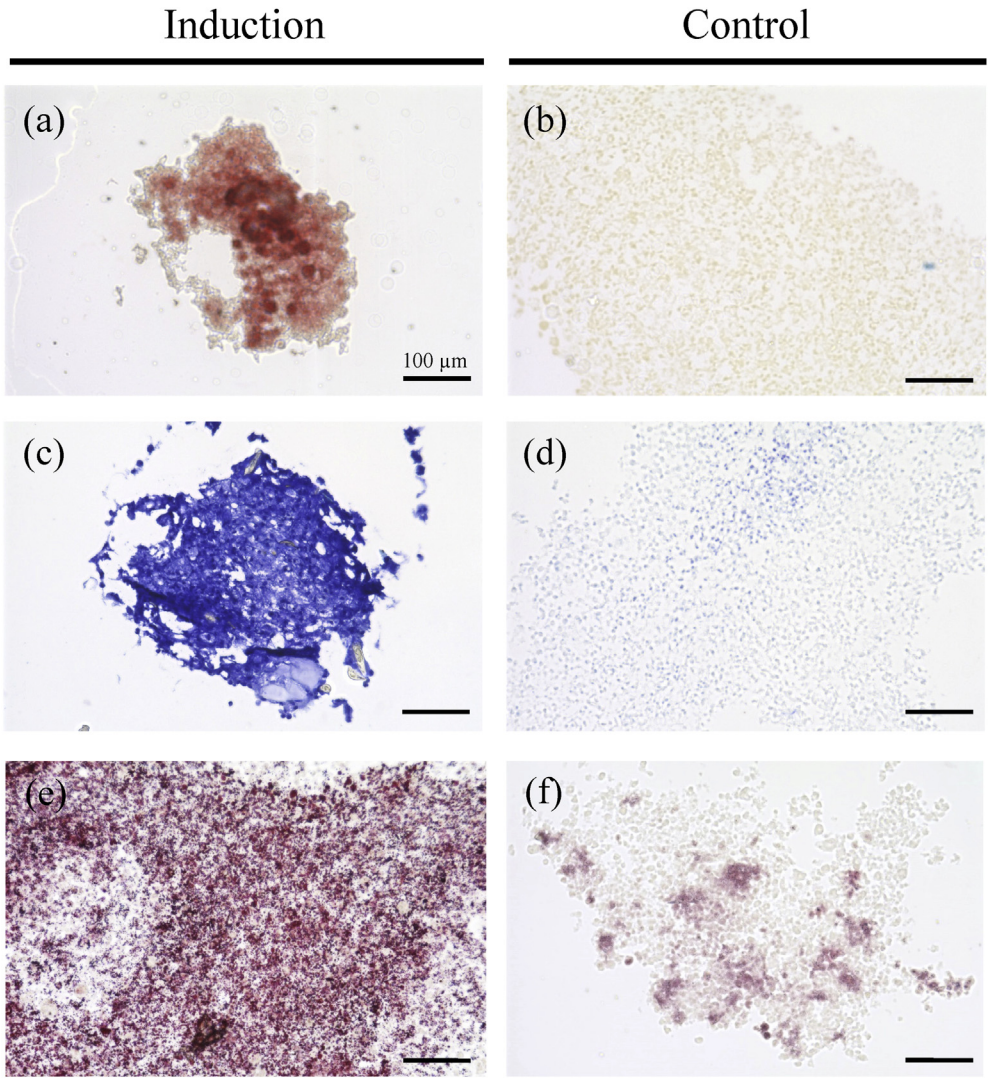

Fig. 4. Tri-linage differentiation of AT-MSC aggregates. (a) Calcium apatite stained with alizarin red in osteogenic induction (b) AT-MSCs slightly stained orange with alizarin red in negative control. (c) Mucopolysaccharides positively stained with toluidine blue in chondrogenic induction. (d) Their nucleuses stained with alcian blue in negative control. (e) Small lipid vesicles stained positively with oil red O in adipogenic induction. (f) No stained vesicles in a negative control. Scale bars = 100 μm (a–f).

Table 1
Modified 2D-MOCART scores.

Feature		Score
Defect fill	Complete	20
	Hypertrophy	15
	Incomplete >50%	10
	Incomplete <50%	5
	Subchondral bone expose	0
Cartilage interface	Complete	15
	Demarcating border visible	10
	Defect visible <50%	5
	Defect visible >50%	0
Surface	Surface intact	10
	Surface damaged <50% of depth	5
	Surface damaged >50% of depth	0
Adhesion	Yes	5
	No	0
Structure	Homogenous	5
	Inhomogeneous or cleft formation	0
Signal intensity	Normal	30
	Nearly normal	10
	Abnormal	0
Subchondral Lamina	Intact	5
	Not intact	0
Subchondral bone	Intact	5
	Granulation tissue, cyst, sclerosis	0
Effusion	No effusion	5
	Effusion	0
Total		(0–100)

Table 2
ICRS gross grading scale.

Feature		Score
Coverage	>75% fill	4
	50–75% fill	3
	25–50% fill	2
	<25% full	1
	No fill	0
Neocartilage color	Normal	4
	25% yellow/brown	3
	50% yellow/brown	2
	75% yellow/brown	1
	100%yellow/brown	0
Defect margins	Invisible	4
	25% circumference visible	3
	50% circumference visible	2
	75% circumference visible	1
	Entire circumference visible	0
Surface	Smooth/level with normal	4
	Smooth but raised	3
	Irregular 25–50%	2
	Irregular 50–75%	1
	Irregular >75%	0
Average		(0–4)

sound cartilage (Fig. 7c). On the other hand, high-intensity signals characteristic of granulomas or fat marrow were pervasive in control defects (Fig. 7d). However, scores based on the modified 2D-MOCART scale were comparable between the two groups (Fig. 8).

3.6. Pathology

Representative macroscopic images are shown in Fig. 9. Gross examination indicated that dense cartilaginous white tissue had covered the surfaces of implanted defects (Fig. 9a) but not control defects (Fig. 9b). Notably, scores for all gross features listed by ICRS were higher in implanted rabbits than in control animals (Fig. 10). In particular, scores for disappearing defect margin were significantly higher in implanted (2.67 ± 0.47) than in control defects (0.0 ± 0.0, $p = 0.001$). Accordingly, average gross scores were significantly higher in the former (2.83 ± 0.12) than in the latter (1.33 ± 0.42, $p = 0.008$).

Representative microscopic images are presented in Fig. 11. Histopathological assessment of implanted defects revealed deposition of a cartilage matrix, as indicated by safranin O staining and immunohistochemistry for type II collagen, as well as formation of subchondral bone (Fig. 11a, c, and e). In contrast, a deeply recessed surface with less bone was observed in control rabbits (Fig. 11b, d, and f). Accordingly, ICRS scores for matrix (2.0 ± 0.0 and 0.66 ± 0.47, $p = 0.016$) and cell distribution (2.0 ± 0.0 and 0.33 ± 0.47, $p = 0.008$) were significantly different between the implanted and control groups (Fig. 12). We note, however, that scores for all features other than cartilage mineralization were higher for implanted defects than for control defects, but not to a statistically significant extent.

Table 3
ICRS histological grading scale.

Feature		Score
Surface	Smooth/continuous	3
	Discontinuities/irregularity	0
Matrix	Hyaline	3
	Mixture; hyaline/fibrocartilage	2
	Fibrocartilage	1
	Fibrous tissue	0
Cell distribution	Columnar	3
	Mixed/columnar clusters	2
	Clusters	1
	Individual cells/disorganized	0
Viability of cell population	Predominantly viable	3
	Partially viable	1
	<10% viable	0
Subchondral bone	Normal	3
	Increased remodeling	2
	Bone necrosis/granulation tissue	1
	Detached/fracture/callus at base	0
Cartilage mineralization (calcified cartilage)	Normal	3
	Abnormal/inappropriate location	0
Average		(0–3)

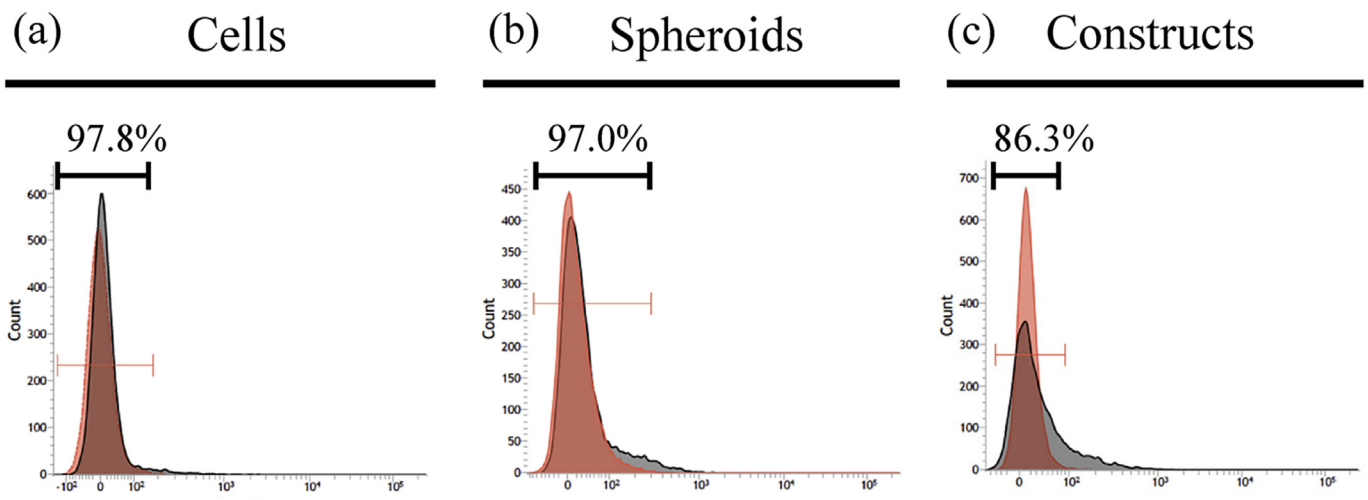

Fig. 5. Cell viability of 2D cultures (a), spheroids (b), and 3D constructs (c). Cell viability is measured as the percentage of cells not stained with PI. Gate was set on unstained samples (red area). Viability was calculated as rate of cells inside of the gate in PI-stained samples (gray area).

Thus, average histological scores were not significantly different between the two groups.

4. Discussion

This study represents the first attempt at osteochondral regeneration using constructs fabricated by a bio 3D printer fitted with a needle array. At first, it was confirmed that the cells obtained from cervical AT had osteogenic, chondrogenic, and adipogenic potential (Fig. 3). Therefore, we defined them as rabbit AT-MSCs. As shown in Fig. 1b, the width of the lumen in constructs just after fabrication was approximately 1.8 mm. However, this width narrowed after extrication from the needle array, and the constructs formed columnar implants (Figs. 1d and 2a). The constructs have moderate hardness and elasticity as confirmed in the section stained with Elastica Masson and by immunohistochemistry of collagen type I (Fig. 6), therefore easy to insert into bone defects during implantation. Importantly, bio 3D printing allows the fabrication of custom grafts with shapes and sizes conforming to individual osteochondral defects. In addition, our results also suggest that implantation of autologous MSCs assembled into 3D constructs may potentially elicit osteochondral regeneration.

Cell viability is reportedly lower inside spheroids than in conventional 2D culture due to necrosis, as spheroids contain more cells which have less access to nutrients [27]. As shown in Fig. 5, the cell viability in the constructs was more than 80%, suggesting that the cells thrived during culture in the needle array. This is presumably because the cells in the needle array were perfused with oxygen and nutrients before extrication. Therefore, we concluded that the methods of cell aggregation and structure fabrication used in this study were useful in overcoming the viability issues reported in 3D cultures. Moreover, it was also confirmed that the cell aggregates indicated osteogenic, chondrogenic, and adipogenic differentiation ability (Fig. 4).

CT imaging suggested that subchondral bone was deposited in defects implanted with the bio 3D-printed constructs (Fig. 7a) but not in untreated defects (Fig. 7b). Similarly, MR imaging suggested that articular cartilage was restored to a state near that of the surrounding normal cartilage in the former (Fig. 7c) but not in the latter (Fig. 7d). These data indicate that the constructs effectively

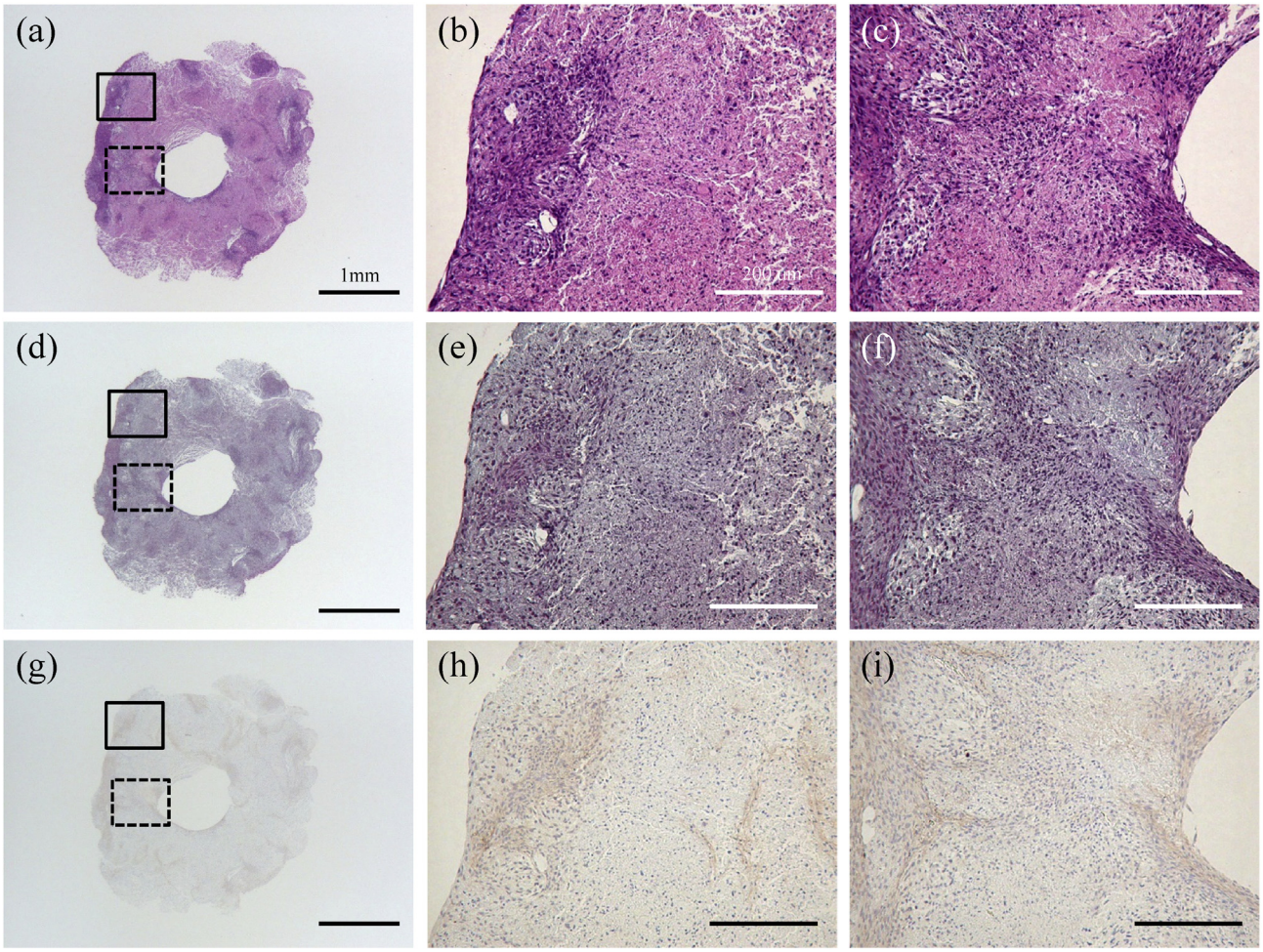

Fig. 6. Microscopic histology. Representative histology of a cell construct, as assessed by hematoxylin & eosin (a, b, and c), Elastica Masson (d, e, and f), and immunohistochemistry for type I collagen (g, h, and i). The defects were implanted with bio 3D printed constructs (a, c, and e) or untreated (b, d, and f). The enlargement of solid squares in a, d, and g are b, e and h, respectively. The enlargement of dotted squares in a, d, and g are c, f and i, respectively. Scale bars in a, d, and g = 1 mm. Scale bars in b, c, e, f, h, and i = 200 μm.

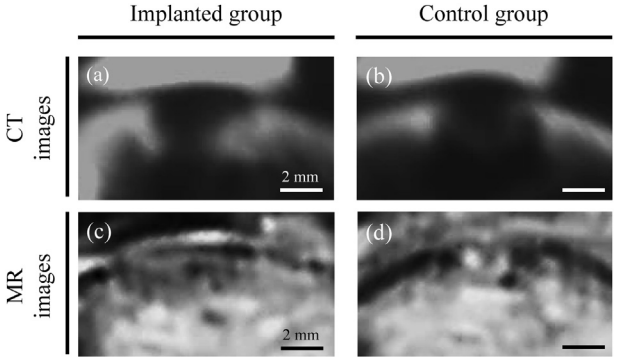

Fig. 7. Observation of bone and cartilage healing by CT and MR imaging. (a and b) Representative CT images of defects treated with bio 3D printed constructs and untreated defects. (c and d) Representative MR images of treated and untreated defects. Scale bars = 2 mm.

repair osteochondral defects. Thus, implantation of these scaffold-free constructs shows promise as a strategy for the regeneration of hyaline cartilage and subchondral bone lost to osteoarthritis.

In particular, MR imaging demonstrated that the double layer of superficial and deep cartilage was nearly restored to normal in treated defects. However, modified 2D-MOCART scores were comparable with those of control animals in all outcome measures (Fig. 8). Thus, these results indicate that while MR imaging may not replace arthroscopy as the gold standard for evaluating cartilage, it may prove a powerful complementary, non-invasive tool not only for assessing injury and matrix degradation due to osteoarthritis [28], but also for assessing bone and cartilage repair after implantation of scaffold-free 3D constructs.

The therapeutic effects of the bio 3D-printed constructs were confirmed by gross examination, upon which implanted defects were found to be abundantly covered with cartilaginous white tissue (Fig. 9a). In contrast, untreated defects remained largely open and barely healed (Fig. 9b). In addition, gross pathology scores for cartilage cover, color, defect margins, and surface smoothness were higher in the former than in the latter (Fig. 10). Indeed, the average ICRS score was significantly higher in treated than in control animals. Collectively, these results indicate that the constructs facilitated repair of osteochondral defects.

Histological features were summarized in Table 4. Formation of cartilage and subchondral bone was observed by microscopic evaluation of defects treated with the bio 3D-printed constructs (Fig. 11a, c, and e). In contrast, less bone formation, deeply recessed surfaces, and fibrous tissue unstained by safranin O were observed in untreated animals (Fig. 11b, d, and f). Accordingly, ICRS histologic scores for all features except cartilage mineralization were higher in

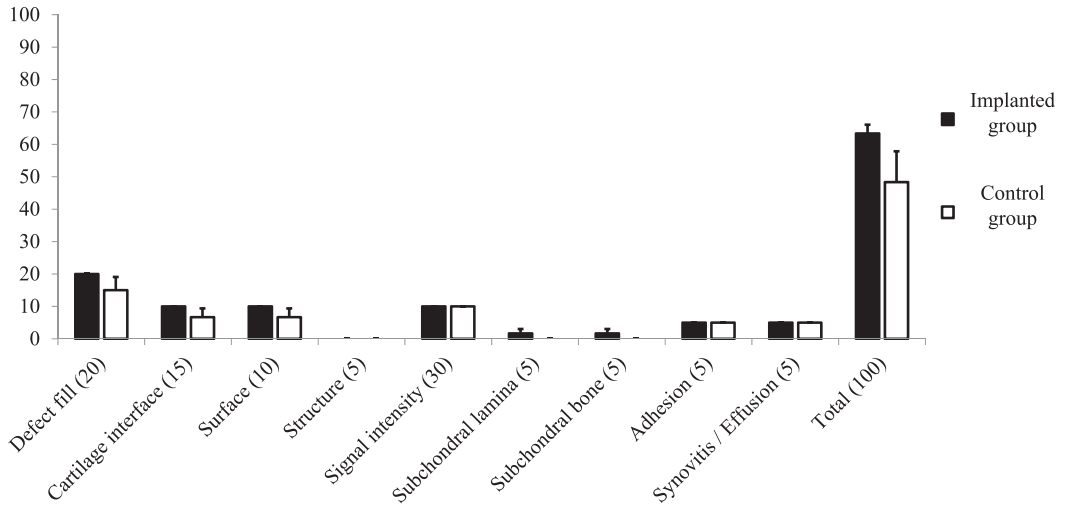

Fig. 8. Modified 2D-MOCART scores of osteochondral defects. There were not significant differences in the outcome measures. $P < 0.05$ was considered to be statistically significant.

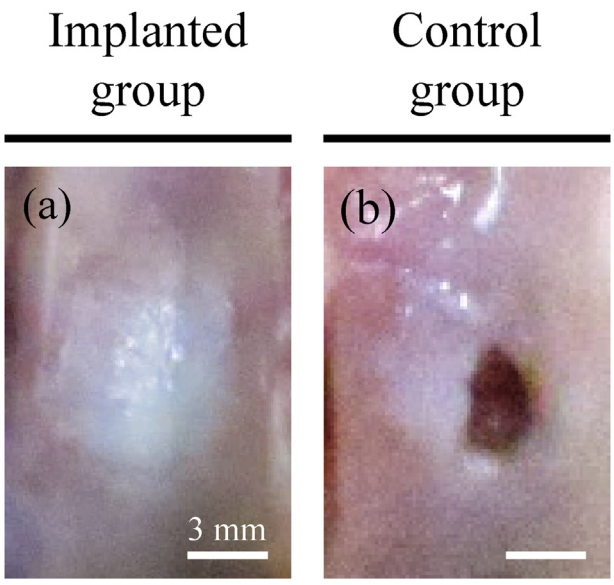

Fig. 9. Gross pathology. Representative gross images of defects treated with bio 3D-printed constructs and untreated defects. Scale bars = 3 mm.

the former than in latter (Fig. 12). In particular, matrix and cell distribution scores were significantly different between the two groups, although the average ICRS histopathological scores were comparable.

However, the formation of subchondral bone is inadequate, and which is reflected in the results of subchondral bone on the ICRS histopathological scores with no significant difference. In our previous report in which a cell construct consisted of AT-MSCs and made using a mold was implanted into osteochondral defects at knee joint in a pig, the construct was firstly differentiated into cartilage, and then the deep layer differentiated into bone undergoing the process of endochondral ossification [23,24]. Accordingly, it can be considered that deep layer of the thick cartilage filling the defect will subsequently differentiate into bone tissue (Fig. 11a, c, and e). Three months may have been insufficient for AT-MSCs construct to progress to endochondral ossification after implantation.

We note, furthermore, that the modified 2D-MOCART scores and histopathological examinations were based only on single 2D sections of 3D tissue. Therefore, cartilage regeneration should be evaluated in three-dimensionally in future experiments, perhaps by 3D-MR imaging as described in previous reports [29,30]. Further, we note that the significant difference in the average ICRS gross

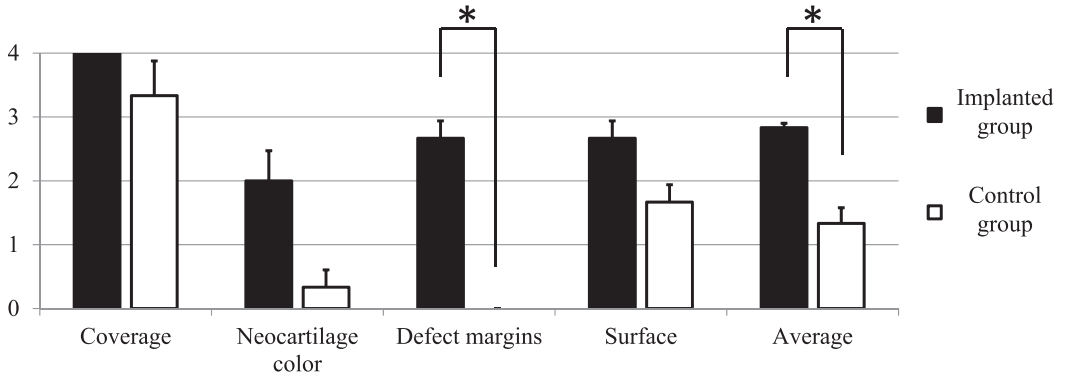

Fig. 10. Macroscopic gross ICRS scores of implanted and control groups with gross ICRS scores. Gross pathology in the implanted group showed significantly (asterisks) higher defect margin and average scores. $P < 0.05$ was considered statistically significant.

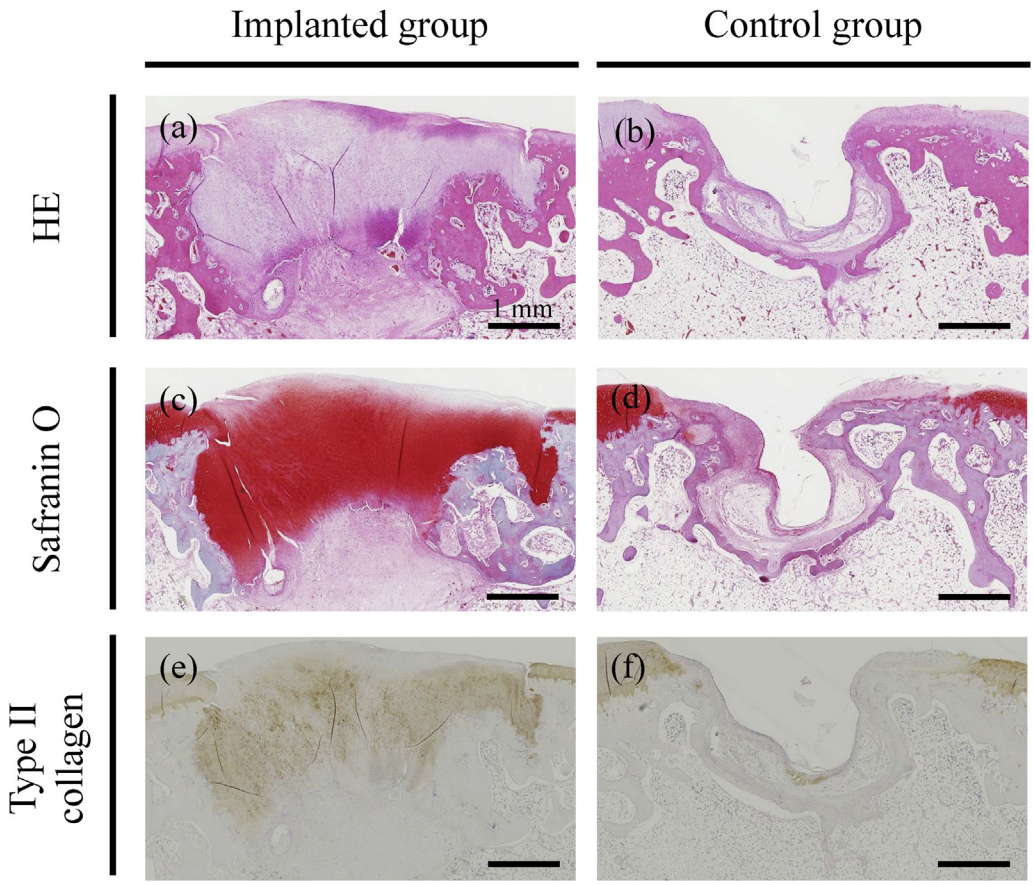

Fig. 11. Microscopic histopathology. Representative histopathology of osteochondral defects, as assessed by hematoxylin & eosin (a and b), safranin O (c and d), and immunohistochemistry for type II collagen (e and f). The defects were implanted with bio 3D printed constructs (a, c, and e) or untreated (b, d, and f). Scale bars = 1 mm.

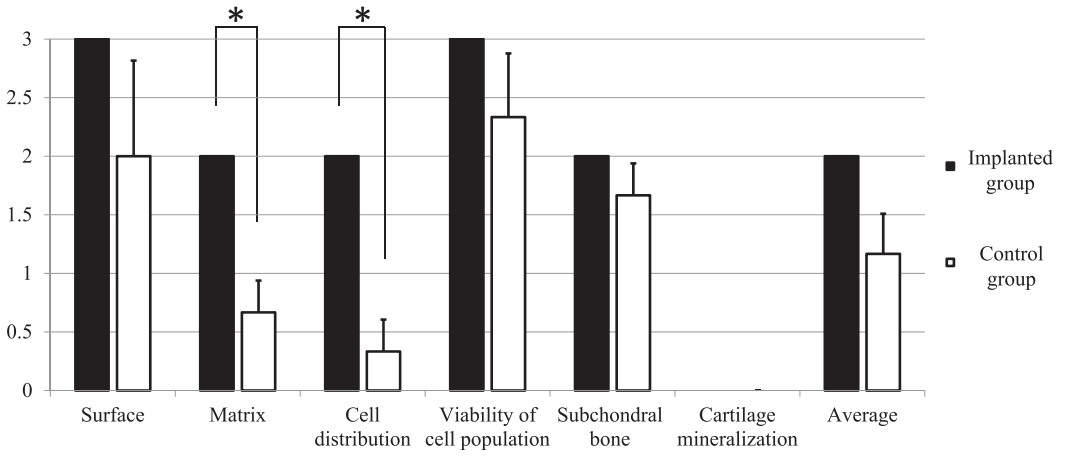

Fig. 12. Microscopic histological ICRS scores of implanted and control groups. Scores of histological outcome measures, such as matrix and cell distribution, were significantly (asterisks) higher in the implanted group than in the control group. $P < 0.05$ was considered statistically significant.

Table 4
Summary of histological features.

Tissue/group name		Bio 3D Printer group	Control group
Cartilage	Surface	Smooth	Irregularity
	Matrix	Mixture; hyaline/fibrocartilage (Transformation)	Fibrocartilage and/or Fibrous tissue
Subchondral bone		Increased remodeling	Bone necrosis and/or Detached

scores definitively demonstrates that scaffold-free 3D construct of AT-MSCs promoted cartilage regeneration (Fig. 10).

Thus far, AT-MSC transplantation for cartilage regeneration has been carried out by intra-articular injection [31,32]. Full-thickness regeneration of articular cartilage and subchondral bone defects has not been reported. The methods in the present study regenerated tissue in defects nearly to the levels of surrounding normal tissue; however, our study was limited by its small number of animal subjects, which affected statistical analysis. Additionally, we only evaluated osteochondral defects at one point during 12-week follow-up period after implantation. CT, MR, and pathological evaluations at 4, 8, 12, 16, or 24-week time points would better track the process of osteochondral regeneration.

The modified 2D-MOCART total scores (Fig. 8) and average ICRS histopathological scores (Fig. 12) in the untreated rabbits were somewhat better than expected. However, the capacity to repair bone persists through life in Rodentia (mice and rats) and lagomorpha (rabbits), but not in humans or other experimental animals, such as pigs, dogs, and horses. Therefore, we speculate that osteochondral defects are more easily repaired in similar rabbits, ultimately resulting in similar modified 2D-MOCART total scores and average ICRS histopathology scores for treated and untreated defects. Therefore, the ability of the scaffold-free bio 3D printed constructs of AT-MSCs to regenerate articular cartilage and subchondral bone should be examined in other experimental animals, such as dogs, pigs, or horses.

5. Conclusions

This is the first report demonstrating that autologous implantation of scaffold-free bio 3D-printed construct into an osteochondral defect regenerates native cartilage and subchondral bone within three months in rabbit.

Author contributions

D.M. prepared the paper, interpreted data, assessed specimens by pathology and histopathology, assessed osteochondral defects by CT and MR, implanted 3D constructs, and obtained AT. Y.K. isolated and expanded AT-MSCs, and prepared 3D constructs on a bio 3D printer and in a mold. K.H. designed and initiated the study, isolated and expanded AT-MSCs, and prepared 3D constructs on a bio 3D printer and in a mold. S.T. assessed osteochondral defects by CT and MR. S.T. assessed the tri-linage differentioaton of AT-MSCs in 2D and 3D. K.N. conceived and supervised the study. All authors approved the final version of the manuscript.

Ethics approval and consent to participate

All procedures were evaluated and approved by the Institutional Animal Care and Use Committee in LSI Medience Corporation (Application No. P130912; Approval No. 2013–0706).

Funding

This study was supported by Japan Society for the Promotion of Science (JSPS) Grant-in-Aid for JSPS Research Fellow Grant Number 19K18503 and funds from Cyfuse Biochemical K.K.

Declaration of competing interest

K.N. is a co-founder and shareholder of Cyfuse Biomedical K.K. Y.K. and K.H. are employees of the same company. The other authors have no commercial, proprietary, or financial interest in the products or companies described in this article.

Acknowledgements

We thank GenoStaff (Tokyo, Japan) and Kureha Special Laboratory (Fukushima, Japan) for performing histological staining and immunohistochemistry. And also, we thank JSPS Grant-in-Aid (JSPS Research Fellow Grant Number 19K18503) and Cyfuse Biochemical K.K for their funds.

Abbreviations

2D	two-dimensional
3D	three-dimensional
AT	adipose tissue
AT-MSCs	adipose tissue-derived mesenchymal stem cells
CCM	complete culture medium
CT	computed tomography
DMEM	Dulbecco's Modified Eagle's Medium
FBS	fetal bovine serum
ICRS	International Cartilage Repair Society
MOCART	magnetic resonance observation of cartilage repair tissue
MR	magnetic resonance
MSCs	mesenchymal stem cells
PBS	phosphate-buffered saline
PI	propidium iodide
PD	proton density
SD	standard deviation

References

[1] Muraki S, Oka H, Akune T, Mabuchi A, En-Yo Y, Yoshida M, et al. Prevalence of radiographic knee osteoarthritis and its association with knee pain in the elderly of Japanese population-based cohorts: the ROAD study. Osteoarthritis Cartilage 2009;17:1137–43.
[2] Mankin HJ. The response of articular cartilage to mechanical injury. J Bone Joint Surg Am 1982;64:460–6.
[3] Gelber AC, Hochberg MC, Mead LA, Wang NY, Wigley FM, Klag MJ. Joint injury in young adults and risk for subsequent knee and hip osteoarthritis. Ann Intern Med 2000;133:321–8.
[4] Lane JG, Massie JB, Ball ST. Follow-up of osteochondral plug transfers in a goat model: a 6-month study. Am J Sports Med 2004;32:1440–50.
[5] Szerb I, Hangody L, Duska Z, Kaposi NP. Mosaicplasty: long-term follow-up. Bull Hosp Jt Dis 2005;63:54–62.
[6] Bentley G, Biant LC, Carrington RW, Akmal M, Goldberg A, Williams AM, et al. A prospective, randomised comparison of autologous chondrocyte implantation versus mosaicplasty for osteochondral defects in the knee. J Bone Joint Surg Br 2003;85:223–30.
[7] Fujisato T, Sajiki T, Liu Q, Ikada Y. Effect of basic fibroblast growth factor on cartilage regeneration in chondrocyte-seeded collagen sponge scaffold. Biomaterials 1996;17:155–62.
[8] Funayama A, Niki Y, Matsumoto H, Maeno S, Yatabe T, Morioka H, et al. Repair of full-thickness articular cartilage defects using injectable type II collagen gel embedded with cultured chondrocytes in a rabbit model. J Orthop Sci 2008;13:225–32.
[9] Diaz-Romero J, Gaillard JP, Grogan SP, Nesic D, Trub T, Mainil-Varlet P. Immunophenotypic analysis of human articular chondrocytes: changes in surface markers associated with cell expansion in monolayer culture. J Cell Physiol 2005;202:731–42.
[10] Tatebe M, Nakamura R, Kagami H, Okada K. Ueda M Differentiation of transplanted mesenchymal stem cells in a large osteochondral defect in rabbit. Cytotherapy 2005;7:520–30.
[11] Pittenger MF, Mackay AM, Beck SC, Jaiswal RK, Douglas R, Mosca JD, et al. Multilineage potential of adult human mesenchymal stem cells. Science 1999;284:143–7.
[12] Zuk PA, Zhu M, Ashjian P, De-Ugarte DA, Huang JI, Mizuno H, et al. Human adipose tissue is a source of multipotent stem cells. Mol Biol Cell 2002;13:4279–95.
[13] Nimura A, Muneta T, Koga H, Mochizuki T, Suzuki K, Makino H, et al. Increased proliferation of human synovial mesenchymal stem cells with autologous human serum: comparisons with bone marrow mesenchymal stem cells and with fetal bovine serum. Arthritis Rheum 2008;58:501–10.
[14] Jones EA, Crawford A, English A, Henshaw K, Mundy J, Corscadden D, et al. Synovial fluid mesenchymal stem cells in health and early osteoarthritis: detection and functional evaluation at the single-cell level. Arthritis Rheum 2008;58:1731–40.

[15] Romanov YA, Svintsitskaya VA, Smirnov VN. Searching for alternative sources of postnatal human mesenchymal stem cells: candidate MSC-like cells from umbilical cord. Stem Cell 2003;21:105–10.
[16] Erices AA, Allers CI, Conget PA, Rojas CV, Minguell JJ. Human cord blood-derived mesenchymal stem cells home and survive in the marrow of immunodeficient mice after systemic infusion. Cell Transplant 2003;12:555–61.
[17] Zuk PA, Zhu M, Mizuno H, Huang J, Futrell JW, Katz AJ, et al. Multilineage cells from human adipose tissue: implications for cell-based therapies. Tissue Eng 2001;7:211–28.
[18] De Ugarte DA, Morizono K, Elbarbary A. Comparison of multi-lineage cells from human adipose tissue and bone marrow. Cells Tissues Organs 2003;174:101–9.
[19] Cukierman E, Pankov R, Stevens DR, Yamada KM. Taking cell-matrix adhesions to the third dimension. Science 2001;294:1708–12.
[20] Baraniak PR, McDevitt TC. Scaffold-free culture of mesenchymal stem cell spheroids in suspension preserves multilineage potential. Cell Tissue Res 2012;347:701–11.
[21] Rettinger CL, Fourcaudot AB, Hong SJ, Mustoe TA, Hale RG, Leung KP. In vitro characterization of scaffold-free three-dimensional mesenchymal stem cell aggregates. Cell Tissue Res 2014;358:395–405.
[22] Ishihara K, Nakayama K, Akieda S, Matsuda S, Iwamoto Y. Simultaneous regeneration of full-thickness cartilage and subchondral bone defects in vivo using a three-dimensional scaffold-free autologous construct derived from high-density bone marrow-derived mesenchymal stem cells. J Orthop Surg Res 2014;9:98.
[23] Murata D, Tokunaga S, Tamura T, Kawaguchi H, Miyoshi N, Fujiki M, et al. A preliminary study of osteochondral regeneration using a scaffold-free three-dimensional construct of porcine adipose tissue-derived mesenchymal stem cells. J Orthop Surg Res 2015;10:35.
[24] Murata D, Akieda S, Misumi K, Nakayama K. Osteochondral regeneration with a scaffold-free three-dimensional construct of adipose tissue-derived mesenchymal stem cells in pigs. Tissue Eng Regen Med 2017;15:101–13.
[25] Nakayama K. In vitro biofabrication of tissues and organs. In: Forgacs G, Sun W, editors. Biofabrication: micro- and nano-fabrication, printing, patterning and assemblies. Oxford: William Andrew; 2013. p. 1–21.
[26] Itoh M, Nakayama K, Noguchi R, Kamohara K, Furukawa K, Uchihashi K, et al. Scaffold-free tubular tissues created by a bio-3D printer undergo remodeling and endothelialization when implanted in rat aortae. PloS One 2015;10:e0136681.
[27] Anada T, Fukuda J, Sai Y, Suzuki O. An oxygen-permeable spheroid culture system for the prevention of central hypoxia and necrosis of spheroids. Biomaterials 2012;33:8430–41.
[28] Goebel L, Orth P, Müller A, Zurakowski D, Bücker A, Cucchiarini M, et al. Experimental scoring systems for macroscopic articular cartilage repair correlate with the MOCART score assessed by a high-field MRI at 9.4 T–comparative evaluation of five macroscopic scoring systems in a large animal cartilage defect model. Osteoarthritis Cartilage 2012;20:1046–55.
[29] Wang YX, Griffith JF, Ahuja AT. Non-invasive MRI assessment of the articular cartilage in clinical studies and experimental settings. World J Radiol 2010;28:44–54.
[30] Hani AF, Kumar D, Malik AS, Ahmad RM, Razak R, Kiflie A. Non-invasive and in vivo assessment of osteoarthritic articular cartilage: a review on MRI investigations. Rheumatol Int 2015;35:1–16.
[31] Toghraie F, Chenari N, Gholipour M, Faghih Z, Torabinejad S, Dehghani S, et al. Treatment of osteoarthritis with infrapatellar fat pad derived mesenchymal stem cells in rabbit. Knee 2011;18:71–5.
[32] Desando G, Cavallo C, Sartoni F, Martini L, Parrilli A, Veronesi F, et al. Intra-articular delivery of adipose derived stromal cells attenuates osteoarthritis progression in an experimental rabbit model. Arthritis Res Ther 2013;15:R22.